Traffic & Transportation

Fatigue driving detection method based on IPPG technology

Jiu-Ju BI[1], Xun-Peng QIN[2], Dong-Jin HU[3], Chen-Yang XU[4]

Original Scientific Paper
Submitted: 24 Nov. 2022
Accepted: 26 Apr. 2023

[1] 1456502465@qq.com, Hubei Key Laboratory of Advanced Technology of Automotive Components, Wuhan University of Technology

[2] 2034175177@qq.com, Hubei Key Laboratory of Advanced Technology of Automotive Components, Wuhan University of Technology

[3] 997858609@qq.com, Hubei Key Laboratory of Advanced Technology of Automotive Components, Wuhan University of Technology

[4] 865347945@qq.com, Hubei Key Laboratory of Advanced Technology of Automotive Components, Wuhan University of Technology

Publisher:
Faculty of Transport and Traffic Sciences, University of Zagreb

ABSTRACT

Physiological signal index can accurately reflect the degree of fatigue, but the contact detection method will greatly affect the driver's driving. This paper presents a non-contact method for detecting tired driving. It uses cameras and other devices to collect information about the driver's face. By recording facial changes over a period and processing the captured video, pulse waves are extracted. Then the frequency domain index and nonlinear index of heart rate variability were extracted by pulse wave characteristics. Finally, the experiment proves that the method can clearly judge whether the driver is tired. In this study, the Imaging Photoplethysmography (IPPG) technology was used to realise non-contact driver fatigue detection. Compared with the non-contact detection method through identifying drivers' blinking and yawning, the physiological signal adopted in this paper is more convincing. Compared with other methods that detect physiological signals to judge driver fatigue, the method in this paper has the advantages of being non-contact, fast, convenient and available for the cockpit environment.

KEYWORDS

vehicle safety system; active safety system; intelligent vehicle; fatigue detection; imaging photoplethysmography.

1. INTRODUCTION

Fatigue driving is one of the main causes of road traffic accidents. Fatigue driving refers to the phenomenon that drivers tend to decrease their driving skills due to mental and physiological disorders caused by the need to continuously perform various mental and physical tasks when driving a vehicle for a long time [1]. It is not a manifestation of human pathology, but a normal physiological activity. With the increase of mental load and physical load, the function of various cells, tissues and organs of the human body will weaken. Currently, the activity of the human sympathetic nerve becomes weak, and the activity of the parasympathetic nerve becomes strong. These reactions cause changes in physiological signals and behaviour. Therefore, physiological indicators can accurately reflect the degree of fatigue. In recent years, with the continuous improvement of people's living standards of traffic safety awareness, it has become very important to identify the driver fatigue driving state.

Research shows that [2], drivers' physiological indexes will deviate from the normal state under fatigue. Therefore, the fatigue state of the driver can be detected according to the changes of physiological signals such as Electromyogram (EMG), Electro-Oculogram (EOG), Electrocardiogram (ECG), electroencephalogram (EEG) and pulse of the driver. For example, Hostens et al. [3] adopted the evoked potential method. When driver fatigue occurs during a long drive, the amplitude of surface EMG increases, while the average frequency decreases. Calcagnini et al. [4] found that four typical features of ECG signals were significantly different between awake and tired states, which are low frequency (LF) energy, ultra-low frequency (VFH) energy, high frequency (HF) energy and the ratio of low frequency energy to high frequency energy. These features can be used to show whether the driver is in a state of fatigue. Ohsuga et al. [5] obtained EOG waveforms under

various mental states according to the relationship among the three parameters of EOG: peak amplitude, rise time and fall time. Lal et al. [6, 7] found the relationship between EEG and driving fatigue through EEG tests: with the deepening of fatigue, the average values of δ and θ relative power spectra of EEG signals gradually increased, while the average values of α and β relative power spectra gradually decreased. The mean values of the relative power spectra of δ, θ and α waves are enhanced at very deep fatigue.

In general, although EMG is objective and authentic, it is invasive to the driver's skin, which is not conducive to the driver's safe driving. The test accuracy of the EOG signal is higher, but the instrument is more complex, and it may interfere with the driver's line of sight during driving. EEG signals can directly and accurately reflect the state of the brain itself, but they are not convenient to carry. The physiological signal detection method based on photoplethysmography (PPG) has been widely used due to its low cost and convenient operation. However, the traditional PPG technology mainly uses sensors to contact the human body to obtain information, which will also bring inconvenience to the driver. The use of non-contact method to detect vital signs is convenient and fast, and more and more researchers pay attention to it. Although human heart rate can be detected by non-contact using LiDAR [8], microwave Doppler radar [9, 10], ultrasound [11] and thermal imaging [12, 13], the systems constructed by these methods are complex and expensive, hence difficult to apply to the specific scene of cockpit.

This paper uses Imaging Photoplethysmography (IPPG) to detect driving fatigue. IPPG [14] technology is a non-contact physiological parameter detection technology developed based on PPG. It uses cameras and other equipment to collect the driver's face information, record the facial changes over a period, and process the captured video to extract pulse waves, and then extract the heart rate variability index by pulse wave characteristics, and finally judge whether the driver is tired according to the index. Compared with the non-contact detection method through identifying drivers' blinking and yawning, the physiological signal adopted in this paper is more convincing. Compared with other methods that detect physiological signals to judge driver fatigue, the method in this paper has the advantages of being non-contact, fast, convenient and available for the cockpit environment.

2. THE USE OF THE IPPG TECHNOLOGY TO EXTRACT THE PULSE WAVE

2.1 The IPPG principle

The basic principle of the IPPG is the Lambert-Beer law and light scattering theory [15, 16]. The Lambert-Beer law states that the concentration of an analyte is directly proportional to the amount of the light absorbed. It also shows that the absorbance of light is not necessarily related to the intensity of light. In the case of a given light wavelength, the absorbance of light is only related to the nature of the medium itself, that is, under the same illumination condition, the absorption degree of the medium with the same thickness is proportional to the concentration of the medium. The Lambert-Beer law is expressed as follows:

$$T = \frac{I}{I_0} \tag{1}$$

$$A = ln\frac{}{T} = K \cdot C \cdot L \tag{2}$$

where A refers to the degree of light absorption by the medium; I_0 is the intensity when the light enters the medium, I is the intensity after the light passes through the medium, T is the ratio of I and I_0, $1/T$ represents the transmittance of the medium; K is the absorption coefficient of the medium, which is determined by the wavelength of the incident light and the properties of the medium itself, C is the concentration of the medium. L is the distance the light travels through the medium. When a medium is irradiated by incident light with intensity I, the intensity of transmitted light passing through the medium can be expressed by *Equation 3*:

$$I = I_0 \cdot e^{-K \cdot C \cdot L} \tag{3}$$

In the case of IPPG, the medium refers to the human skin tissue. Since the absorption of light by venous blood and other tissues in the skin basically does not change, only the absorption of light by arterial blood is considered. When the heart diastoles, the volume of blood in the blood vessels decreases, the volume of blood becomes smaller, and the distance of light passing through decreases accordingly. Currently, the skin absorbs the least amount of light, and the intensity of light passing through the tissue is the highest. Let the distance at

this time be L_{min} and the absorption degree of light be A_{min}, then the light intensity at this time can be expressed as:

$$A_{min} = K \cdot C \cdot L_{min} \tag{4}$$

Accordingly, when the heart contracts, the volume of blood in the blood vessels reaches the maximum, and the volume of blood increases, causing the distance of light through the tissue to be larger, and the skin absorption at that moment is the lightest, whereas the intensity of light coming through is the lowest. Let the distance at this time be L_{max} and the absorption degree of light be A_{max}, then the light intensity at this time can be expressed as:

$$A_{max} = K \cdot C \cdot L_{max} \tag{5}$$

Make the difference between the above two formulas to obtain:

$$\Delta A = K \cdot C \cdot \Delta L \tag{6}$$

Equation 6 shows that when the incident light is constant, the absorption degree of human skin tissue to light is only related to the volume of arterial blood, and the change of the absorption degree is proportional to the change of the volume of blood. Therefore, if the change of skin surface light is detected, the change of blood volume can be obtained, as well as the waveform of the human pulse wave.

2.2 Extraction of the pulse wave

The main steps are as follows: first, screen and edit the collected videos, eliminate the nonstandard videos. Second, frame image separation is carried out on the experiment video data. After this, the video will be transformed into 30 images per second. Third, use the face detection algorithm to detect the face of the video data separated from the frame image. Fourth, select an appropriate region of interest (ROI) and separate the primary colour of the ROI into three colour channels, R, G and B, and calculate the mean of the pixel values of the three-color channels of each ROI. Fifth, the heart rate signal is separated from the above RGB channels by blind source separation technology. Finally, filtering operations are carried out on the data obtained in the fifth step to filter out the mixed noise. The technical route of pulse wave extraction based on the IPPG technology is shown in *Figure 1*.

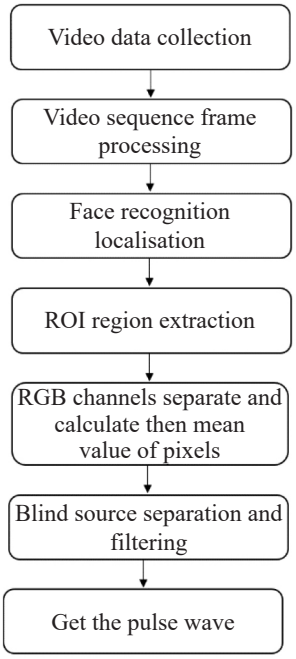

Figure 1 – Technology roadmap

In practice, the experiment video contains not only the parts of the human body to be detected, but also the irregular background. The imaging size and angle of the detection site will also be changed with the body shaking. These factors will reduce the noise ratio of the signal, so it is necessary to process the video to get the image sequence of the detected part.

In theory, the skin of any part of the human body can be used as the detection area, but in the specific experiment, the convenience of operation and the distribution of human blood vessels should be given priority. The area should be easy photograph and to distribute with as many blood vessels as possible. From *Figure 2*, there are many capillaries distributed on the face. The subjects simply need to sit in front of the monitor and make sure their heads are fully presented in the laptop camera. Based on the above considerations, the facial region was selected as the region of interest of the human body.

When the facial region is selected as the ROI, the eye region is removed in the experiment as the unconscious actions such as blinking will produce large motion spurious errors and bring non-negligible noise to the experimental results, as shown in *Figure 3*.

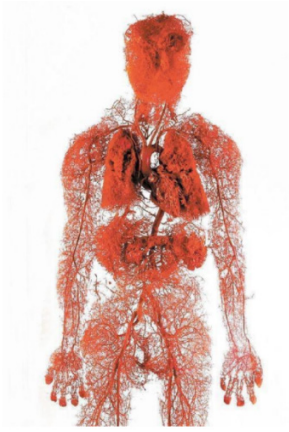

Figure 2 – Human vascular distribution

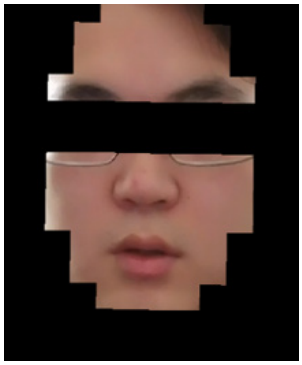

Figure 3 – Schematic diagram of ROI region extraction

Pulse wave signal is obtained by calculating the grey mean of the image of the region of interest, and then separating and filtering the data blind source. The calculation formula of the grey mean is as follows:

$$X(t)=\frac{\sum_{i=1}^{i=M}\sum_{j=1}^{j=N}x(i,j,t)}{M\cdot N} \tag{7}$$

where, M represents the length of the picture, N represents the width of the picture, and $x(i,j,t)$ represents the grey value of each pixel.

The grey mean of R, G and B channels of each frame of the ROI image is calculated and the result is shown in *Figure 4*.

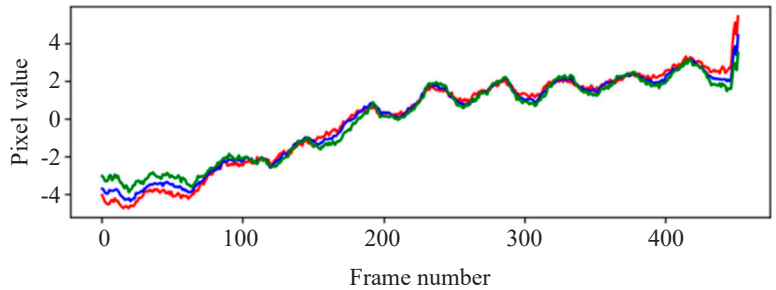

Figure 4 – Grey mean of RGB three-channel

During the experiment, the external light influence, or the interference of the imaging equipment itself, may cause interference to the extracted source pulse wave signal. Because it is impossible to know whether the noise mixed in the source pulse wave signal is additive or multiplicative, it is impossible to filter the source pulse wave signal directly through the filter. In this case, Blind Source Separation (BSS) techniques can be used to solve the problem [17].

In addition to the required source signal, there are also some unknown signals in the original signal. At this time, the observation of the original signal is obtained by equipment or instrument, and the observation is used as the input to realise the original signal estimation. The solution method is blind source separation, which is mainly applied to the processing of digital signals [18]. The most important characteristic of blind source

separation is that it cannot only estimate the signal, but also ensure that the periodic information of the signal is not lost [19].

Independent component analysis (ICA), as a commonly used blind source separation technology, is widely used in the field of artificial intelligence, biomedicine [20] and industry. The Principal Component Analysis (PCA) method guarantees that the decomposed signal components are not correlated, but cannot guarantee that these components are independent. The ICA algorithm is aimed at independent component decomposition. PCA requires data to conform to a certain distribution, such as the Gaussian distribution. But the ICA does not have that requirement. Therefore, the ICA is used for the blind source separation of signals in this paper. The prerequisite of the ICA method is to reduce the correlation between signals and keep the independence of signal data as far as possible. The main principle of the ICA is to solve the real source signal S and mixing matrix K to be separated by processing the observed source signal X accordingly, where the relationship between them is shown in *Equation 8*:

$$X = K \cdot S \tag{8}$$

In general, S cannot be accurately solved. The matrix N can be solved by using the auxiliary separation matrix L. In this case, N can be used as an approximate estimate of the real source signal S and its relation is shown in *Equation 9*:

$$N = L \cdot X \tag{9}$$

The FastICA method in the ICA model is adopted in this paper, which was proposed by Hyvarinen et al in 1999 and has the characteristics of parallel computing and low memory consumption [21]. This algorithm is an iterative algorithm to quickly find the optimal solution. Compared with the common ICA algorithm, the convergence speed is fast. Compared with gradient-based algorithm, Fast ICA does not need to select step parameters, indicating that the algorithm is easier to use. Fast ICA can directly find any non-Gaussian independent component by using a nonlinear function. For other algorithms, they must first estimate the probability density distribution function and then make nonlinear selection accordingly. In addition, the independent components of the Fast ICA can be estimated one by one, which can greatly reduce the amount of calculation when only a few independent components need to be estimated. Before using this algorithm, it needs to be pre-processed, including centralisation and whitening.

Centralised processing: the mean value of the data to be observed is subtracted from X so that the sample becomes zero mean:

$$\overline{X_i} = X_i - \sum_{j=1}^{m} x_i^{(j)}, \quad i = 1,2,\ldots,n \tag{10}$$

Whitening treatment: Usually, data covariance is processed by eigenvalue decomposition during whitening treatment. Here, the signal is simply multiplied by a whitening matrix:

$$Z = V \cdot X \tag{11}$$

After solving and calculating, the relatively independent real physiological characteristic signal S can be estimated. The independent components corresponding to the three channels R, G and B can be obtained by the FastICA calculation and analysis of the above processed data. This is shown in *Figure 5*.

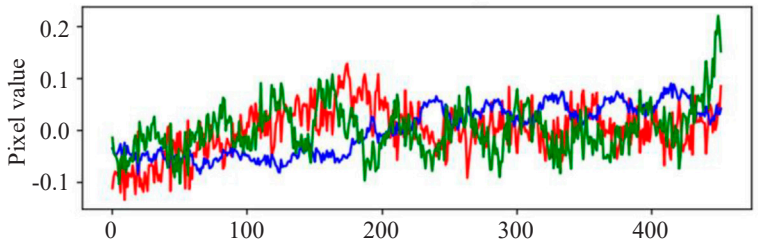

Figure 5 – ICA recovered signals

The signal in the G channel best reflects the pulse wave. This is because the highest degree of absorption of visible light is in the range of 510 nm to 590 nm. This wavelength range corresponds to yellow-green light,

so the blood has the highest degree of absorption of yellow-green light. Pulse wave signal can be obtained by filtering the signal of G channel.

To use Image filtering, image will be suppressed or the noise eliminated without damaging the important information. The quality of the image will be affected by the noise produced in the process of image acquisition and signal transmission. The external environment is an important factor to image quality, such as the excessive light, insufficient light and light pollution. In addition, the stability of the data acquisition equipment itself, as well as the data distortion or loss in the process of data transmission, are also factors that cannot be ignored. Image filtering will greatly influence the subsequent experimental analysis.

The range of human heart rate is 50 bmp to 220 bmp. By converting the frequency range, it is about 0.8 Hz to 3.8 Hz, the band pass filter is used to filter the frequency outside the range, which can effectively eliminate the noise. The signal waveform after bandpass filtering is shown in *Figure 6*. Most of the noise has been filtered out. Compared with before processing, the signal curve becomes smoother and the signal periodicity after processing is more obvious.

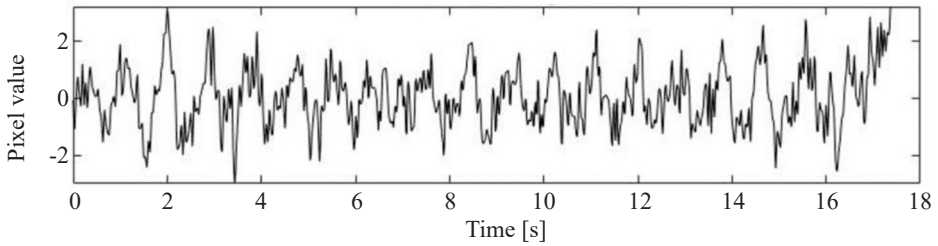

Figure 6 – Pulse wave signal

3. EXTRACTED HEART RATE VARIABILITY INDEX BASED ON PULSE WAVE

3.1 Heart rate variability

Heart rate variability is the change in the difference between heart cycles. Heart rate variability is considered to reflect the activity of the autonomic nervous system and its influence on the cardiovascular system, since the heart beats by the autonomic nervous system to control the pacing of the sinus node and drive the contraction and relaxation of the whole heart. In medicine, heart rate variability is thought to reflect the coordination of sympathetic and vagus nerves in the heart. Reduced sympathetic activity or increased vagal activity can lead to reduced heart rate variability. Therefore, HRV is related to many physiological phenomena, and can be used to judge the rehabilitation of a variety of cardiovascular diseases [22], as well as to measure the health status of the general population, the ability of athletes to adapt to stress and whether drivers are tired-driving [23].

In this paper, firstly, the collected and pre-processed pulse wave signal is extracted for the time interval and the pulse wave time interval sequence is obtained. For the pulse wave intertemporal sequence, three methods can be used: time domain analysis, frequency domain analysis and nonlinear index analysis. When time-domain analysis is used for the heart rate variability analysis, its accuracy mainly depends on the length of the analysis recording time interval, so there is a large error for time-domain analysis in a short period. Therefore, this paper mainly adopts the method of combining the frequency domain index of heart rate variability and nonlinear index to detect and analyse human mental fatigue.

3.2 Analysis of the heart rate variability in frequency domain

Frequency domain analysis is a very effective and practical method for digital signal processing, which can be used to process periodic signals. Because pulse signal is a periodic signal, it can also be processed by frequency domain analysis. At present, the frequency domain analysis of the pulse wave is usually based on power spectrum. The application of power spectrum analysis to pulse can provide an auxiliary reference for disease diagnosis. In different frequency bands, the energy of human pulse wave is significantly different between normal state and fatigue state. Therefore, the spectral energy ratio of different frequency bands is usually used as the frequency domain characteristic when analysing the mental fatigue state based on pulse wave.

The frequency domain index analysis of heart rate variability is mainly based on the analysis of self-signal power spectral density (PSD), which is used to measure how the power is distributed with frequency. The power spectral density can be calculated by a variety of mathematical methods. The most common methods

include Welch, Blackman-Tukey and Lomb-Scargle periodograms and autoregressive modelling. The frequency domain analysis method of the Welch power spectrum diagram is simple and efficient, while the calculation process of the other analysis methods is complicated, long and obtaining data is very time consuming. Therefore, the Welch power spectrum diagram is used for frequency domain analysis in this paper.

The Welch power spectrogram is obtained by first dividing the resampled sequence and windowing each segment to reduce the leakage effect. The frequency estimation is obtained by averaging the Fast Fourier Transform (FFT) spectrum at the window end. The Welch's processing method is as follows: the obtained RRI is divided into *L* segments, each with a length of *M*, and each segment is allowed to overlap by half.

$$L = \frac{N - M/2}{M/2} \tag{12}$$

The data in paragraph *i* are labelled as follows:

$$X_N^i(n) = X_N\left[n + (i+1)M/2\right],\ 0 \le n \le M-1,\ 1 \le i \le L \tag{13}$$

Calculate the power spectrum of each segment of data:

$$P_{PER}^i(k) = \frac{1}{M \cdot U}\left|\sum_{n=0}^{M-1} x_N^i(n) W(n) e^{-j2\pi kn/M}\right|^2,\ 0 \le k \le M-1 \tag{14}$$

The data analysed in the frequency domain include the normalised components of High Frequency (HF) and Low Frequency (LF), which respectively represent the percentage of HF in HF+LF and the percentage of LF in HF+LF. The calculation formula is as follows:

$$HF_{norm} = \frac{HF}{TP - VLF} \cdot 100\% \tag{15}$$

$$LF_{norm} = \frac{LF}{TP - VLF} \cdot 100\% \tag{16}$$

Total Power (TP) represents the sum of HRV power in the frequency domain. Generally speaking, the frequency of Very Low Frequency (VLF) is set at 0.003-0.04 Hz, the frequency of LF is set at 0.04–0.15 Hz and the frequency of HF is set at 0.15–0.4 Hz. Physiologically, the LF frequency band is associated with parasympathetic stimulation of the autonomic nervous system and the HF frequency band is associated with sympathetic stimulation of the autonomic nervous system [24].

3.3 Analysis of nonlinear indicators of heart rate variability

The nonlinear index of heart rate variability can be used to help describe the more complex cardiac dynamics in the process of cardiovascular regularisation, while the linear index cannot complete this complex process, so the nonlinear analysis of heart rate variability can effectively make up for the deficiency of linear analysis in this aspect [25]. Since the 1980s, with the rapid development of nonlinear dynamics, the nonlinear analysis method of HRV has made a lot of progress. At present, HRV nonlinear analysis methods can be divided into graphic method and nonlinear parameter calculation method. The graphic method is mainly Poincare scatter diagram analysis. Fractal dimension analysis method, complexity analysis method, Lyapunov index, Kolmogorov entropy or measure entropy, approximate entropy analysis and so on are commonly used to calculate nonlinear parameters, which are all quantitative methods of nonlinear analysis. At present, scatter plot method is the most studied method and other methods are mostly limited to the theoretical stage, lack of clinical application and insufficient research.

The nonlinear index analysis in this paper uses the Poincare Plot based on the RR interval, which represents the correlation between the RR intervals as a scatterplot, which is a projection of the reconstructed attractor describing the dynamics of the cardiac system.

It takes RRn/ms as the abscissa and RRn+1/ms as the ordinate and displays a line composed of scattered points along a certain direction. Each Poincare scatter diagram drawn based on the RR interval can make a corresponding ellipse on the scatter line, whereas points perpendicular to and along the scatter line are the width and length of the ellipse. They are determined by the standard deviations SD1 and SD2, with SD1 reflecting

the short-term variability and SD2 reflecting the long-term variability [26]. For the convenience of calculation, the coordinate system of the figure is rotated counter clockwise. In the rotating coordinate system [27],

$$\begin{bmatrix} x_1 \\ x_2 \end{bmatrix} = \begin{bmatrix} \cos\theta & -\sin\theta \\ \sin\theta & \cos\theta \end{bmatrix} \begin{bmatrix} RR_n \\ RR_{n+1} \end{bmatrix} \tag{17}$$

$$SD_1 = D(x_1) = D\left(\frac{\sqrt{2}}{2}RR_n - \frac{\sqrt{2}}{2}RR_{n+1}\right) = \frac{1}{2}D(RR_n - RR_{n+1}) \tag{18}$$

$$SD_2 = D(x_2) = D\left(\frac{\sqrt{2}}{2}RR_n + \frac{\sqrt{2}}{2}RR_{n+1}\right) = \frac{1}{2}D(RR_n + RR_{n+1}) \tag{19}$$

4. EXPERIMENTAL RESULTS AND ANALYSIS

4.1 Experimental design

In this paper, the author uses Lenovo R9000P laptop as signal acquisition equipment. The processor is AMD Ryzen 7 5800H with Radeon Graphics and the main frequency is 3.2 GHz. Set the camera resolution to 1280×720, the sampling frame rate to 30 fps and the RGB colour depth of the pixel to 24 bits. Matlab software was used for offline data processing of the video.

The author selected 10 graduate students as subjects, age 23 to 27, in good health condition, with no neurological disorders or heart disease. They were numbered A–J and were asked to take two tests. At 8 o'clock, each subject got in the car and ready to drive. In the meantime, the first videos were being recorded. The subjects then drove around the school for four hours, returning to school at 12 o'clock, after which the second batch of videos was recorded. In the video collection process, the subjects sat in front of the computer at about 40cm. The experimental scene was shown in *Figure 7*. The videos were then analysed and the experimental design is shown in *Figure 8*. During the experiment, natural light was used as the incident light source and the sampling time was about 20 seconds.

Figure 7 – Experimental scene of subjects

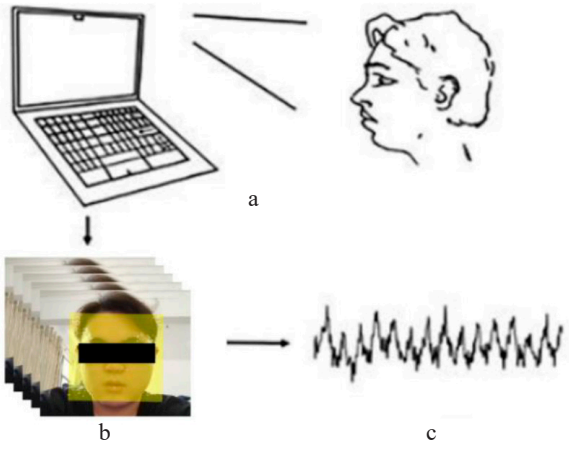

Figure 8 – the experimental design

4.2 Analysis of experimental results in the frequency domain

The frequency domain index of heart rate variability is mainly to analyse the ratio change of low frequency band (LF) power and high frequency band (HF) power. The very low frequency, low frequency and high frequency spectra of volunteers can be obtained from the Welch power spectrum diagram.

In this paper, the pulse wave signals of 10 subjects were divided into two stages, and the LF/HF ratio of 10 subjects was calculated according to the formula. The following figures are the power spectrum density map of one subject during two tests.

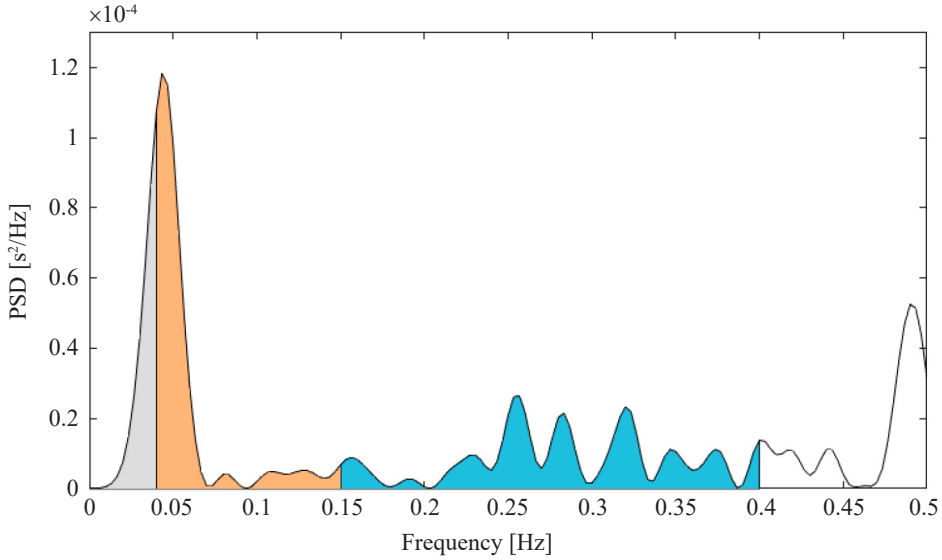

Figure 9 – Power spectral density map of subject A for the first test

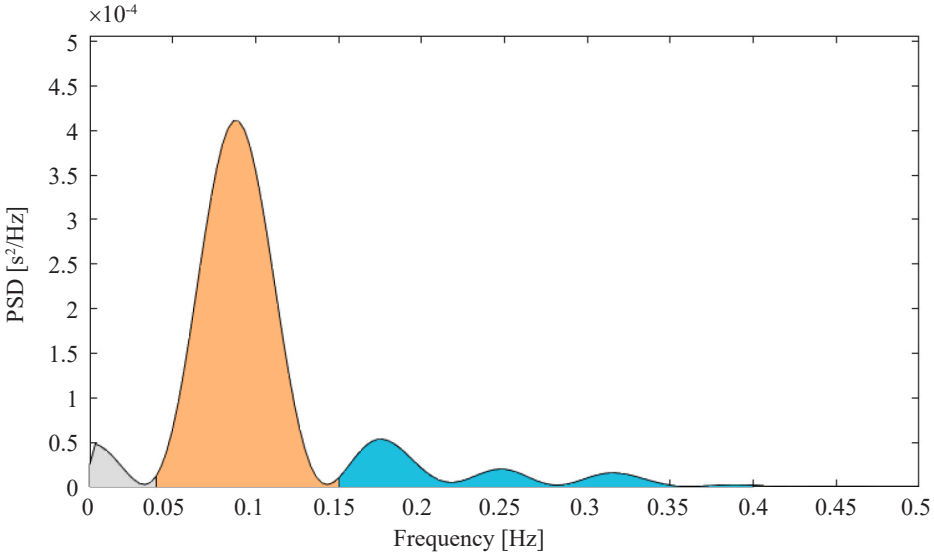

Figure 10 – Power spectral density map of subject A for the second detection

LF/HF values of all subjects are shown in *Table 1*.

Table 1 – Statistical table of frequency domain indexes of 10 subjects

Subject serial number	LF/HF (The first time)	LF/HF (The second time)
A	0.9949	5.8431
B	0.6152	4.4785
C	1.1275	6.5259
D	0.7186	5.3741
E	0.5528	3.9726
F	1.4361	7.5283
G	0.5468	4.3025
H	0.8753	5.1679
I	0.9142	6.2794
J	0.7918	6.1326

The results show that the ratio of LF to HF will increase in the fatigue state. When LF/HF is between 0 and 3, the human body is awake; when LF/HF is greater than 3, the human body is in a state of fatigue [28]. The conclusion is in good agreement with this experiment. Cong Yu Wang et al. proposed a method based on indirect contact electrocardiography. Their experimental results show that the LF/HF index is feasible for evaluating fatigue degree [29]. Chao Zeng et al. extracted the frequency domain index LF/HF from the ECG signals to explore the influence of gender factors on drivers' driving fatigue. The results showed that both men and women experienced and increase in LF/HF [30]. The experimental results and data in the above literatures are consistent with those in this paper.

4.3 Analysis of the nonlinear index of experimental results

In this paper, the pulse wave signals of 10 subjects at two stages were used to calculate the nonlinear indicators SD1 and SD2 of heart rate variability according to the formula. SD1 and SD2 respectively represent the width and length of the ellipse of the Poincare diagram, which can effectively reflect the level of short-term and long-term heart rate variability of the body. The Poincare scatter plot of the RR time interval series of two times for one of the subjects is shown below.

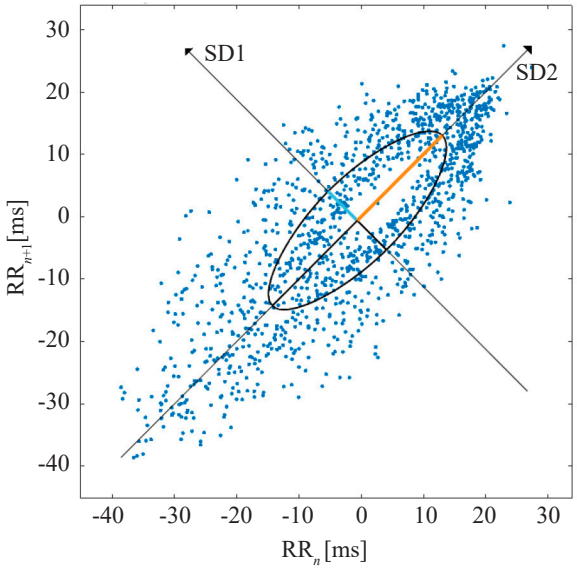

Figure 11 – Poincare scatter plot of Subject A for the first test

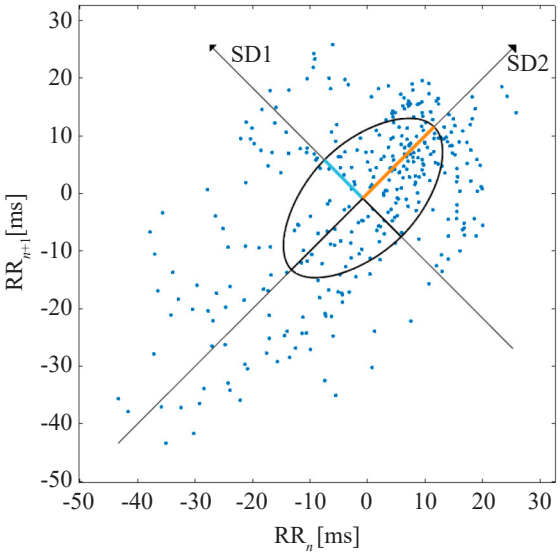

Figure 12 – Poincare scatter plot of Subject A for the second test

Table 2 shows the SD1 and SD2 data after statistical summary by calculation.

Table 2 – Statistical table of nonlinear indexes of 10 subjects

Subject serial number	SD1/SD2 (The first time)	SD1/SD2 (The second time)
A	0.3433	0.5379
B	0.2546	0.4826
C	0.3854	0.5722
D	0.3161	0.5012
E	0.2347	0.4341
F	0.3978	0.5938
G	0.2549	0.4508
H	0.3204	0.4981
I	0.3692	0.5731
J	0.3094	0.4847

The shape of the Poincare scatter plot directly reflects the characteristics of the instantaneous heart rate curve. The scatter chart of the driver under normal condition is comet-like and most of the scatter chart is concentrated near the line at 45° angle in the figure, as shown in Figure 4.5. This suggests that the RR intervals between adjacent sinus beats in drivers are roughly equal. The scatter points in Figure 4.6 spread out around the 45° line, indicating that the driver has sinus arrhythmia and is in a state of fatigue. Studies show that under normal circumstances, the ratio of SD1/SD2 is around 0.25, but when the human body is in a state of mental fatigue, this ratio will show an upward trend and is significantly greater than 0.25 [28]. Laurent Mourot et al. evaluated the effectiveness of the Poincare graph analysis. Their research shows that the Poincare plot parameters as well as the "width" of the scatter plot can be viewed as a substitute for HRV time and frequency domain analysis. Its standard deviation is significantly correlated with the main parameters of the time and frequency domain analysis, especially the parasympathetic indicators. They observed that the Poincare scatter plot was wider when people were fatigued and detailed data were provided to assess changes in human HRV caused by fatigue [31]. The conclusion is in good agreement with this experiment.

5. CONCLUSION

In this paper, camera and other equipment are used to collect the driver's face information, to record the facial changes over a period and process the captured video. The pulse wave is extracted by blind source separation technology and then the frequency domain index and nonlinear index of heart rate variability are extracted by pulse wave sign. Finally, the fatigue of the driver is judged according to the index. According to the result in Chapter 4, when the human body is in a state of fatigue, the frequency domain indices and nonlinear indices show an obvious upward trend, and the fatigue of the human body can be clearly judged according to the relevant literature [28–31]. In this study, the IPPG technology was used to realise non-contact driver fatigue detection to ensure safe and healthy driving. Compared with the non-contact detection method through identifying drivers' blinking and yawning, the physiological signal adopted in this paper is more convincing. Compared with other methods that detect physiological signals to judge driver fatigue, the method in this paper has the advantages of being non-contact, fast, convenient and available for the cockpit environment.

REFERENCES

[1] Mao Zhe. *Research on recognition method of motor vehicle fatigue driving behavior*. PhD Thesis. Wuhan University of Technology, China; 2009. DOI: 10.7666/d.y1653097.

[2] Shen KQ, Li XP, Ong CJ, et al. EEG-based mental fatigue measurement using multi-class support vector machines with confidence estimate. *Clinical Neurophysiology*. 2008;119(7):1524-1533. DOI: 10.1016/j.clinph.2008.03.012.

[3] Hostens I, Ramon H. Assessment of muscle fatigue in low level monotonous task performance during car driving. *Journal of Electromyography and Kinesiology*. 2005;15(3):266-274. DOI: 10.1016/j.jelekin.2004.08.002.

[4] Calcagnini G, et al. Spectral analysis of heart rate variability signal during sleep stages. *Proceedings of 16th Annual International Conference of the IEEE Engineering in Medicine and Biology Society*. Vol. 2. 1994. DOI: 10.1109/IEMBS.1994.415418.

[5] Ohsuga M, et al. Classification of blink waveforms toward the assessment of driver's arousal levels-an EOG approach and the correlation with physiological measures. *Engineering Psychology and Cognitive Ergonomics: 7th International Conference, EPCE 2007, Held as Part of HCI International 2007, Beijing, China, July 22-27, 2007. Proceedings 7*. 2007. DOI: 10.1007/978-3-540-73331-7_86.

[6] Lal SKL, Craig A. Electroencephalography activity associated with driver fatigue: Implications for a fatigue countermeasure device. *Journal of Psychophysiology*. 2001;15(3):183. DOI: 10.1027/0269-8803.15.3.183.

[7] Lal SKL, et al. Development of an algorithm for an EEG-based driver fatigue countermeasure. *Journal of safety Research*. 2003;34(3):321-328. DOI: 10.1016/S0022-4375(03)00027-6.

[8] Ulyanov SS, Tuchin VV. Pulse-wave monitoring by means of focused laser beams scattered by skin surface and membranes. *Static and Dynamic Light Scattering in Medicine and Biology*. 1993;1884:160-167. DOI: 10.1117/12.148363.

[9] Greneker EF. Radar sensing of heartbeat and respiration at a distance with applications of the technology. *Radar 97 (Conf. Publ. No. 449)*. 1997. p. 150-154. DOI: 10.1049/cp:19971650.

[10] Hafner N, Drazen JC, Lubecke VM. Fish heart rate monitoring by body-contact Doppler radar. *IEEE Sensors Journal*. 2012;13(1):408-414. DOI: 10.1109/JSEN.2012.2210400.

[11] Rabben SI, et al. An ultrasound-based method for determining pulse wave velocity in superficial arteries. *Journal of Biomechanics*. 2004;37(10):1615-1622. DOI: 10.1016/j.jbiomech.2003.12.031.

[12] Garbey M, et al. Contact-free measurement of cardiac pulse based on the analysis of thermal imagery. *IEEE Transactions on Biomedical Engineering*. 2007;54(8):1418-1426. DOI: 10.1109/TBME.2007.891930.

[13] Fei J, Pavlidis I. Thermistor at a distance: Unobtrusive measurement of breathing. *IEEE Transactions on Biomedical Engineering*. 2009;57(4):988-998. DOI: 10.1109/TBME.2009.2032415.
[14] Torres JCC, Abderrahim M. Measuring heart and breath rates by image photoplethysmography using wavelets technique. *IEEE Latin America Transactions*. 2017;15(10):1864-1868. DOI: 10.1109/TLA.2017.8071228.
[15] Hertzman AB. The blood supply of various skin areas as estimated by the photoelectric plethysmograph. *American Journal of Physiology-Legacy Content*. 1938;124(2):328-340. DOI: 10.1152/ajplegacy.1938.124.2.328.
[16] Sinex JE. Pulse oximetry: Principles and limitations. *The American Journal of Emergency Medicine*. 1999;17(1):59-66. DOI: 10.1016/S0735-6757(99)90019-0.
[17] Wei B, Zhang C, Wu X. Comprehensive comparison study on different ICA/BSS methods in IPPG techniques for obtaining high-quality BVP signal. *Proceedings of the 2016 International Conference on Intelligent Information Processing*. 2016. p. 1-6. DOI: 10.1145/3028842.3028890.
[18] Li S, Guo H, Li D. Vibration signal processing method review. *Journal of Instruments and Meters*. 2013;(8):1907-1915. DOI: 10.19650/j.cnki.cjsi.2013.08.031.
[19] Yang Z, Li Y, Hu D. Review of independent component analysis methods. *Acta Automatica Sinica*. 2002;(05):762-772. DOI: 10.16383/j.aas.2002.05.012.
[20] James CJ, Hesse CW. Independent component analysis for biomedical signals. *Physiological Measurement*. 2004;26(1):R15. DOI: 10.1088/0967-3334/26/1/R02.
[21] Hyvarinen A. Fast and robust fixed-point algorithms for independent component analysis. *IEEE Transactions on Neural Networks*. 1999;10(3):626-634. DOI: 10.1109/72.761722.
[22] Pinheiro N, et al. Can PPG be used for HRV analysis?. *2016 38th Annual International Conference of the IEEE Engineering in Medicine and Biology Society (EMBC)*. 2016. p. 2945-2949. DOI: 10.1109/EMBC.2016.7591347.
[23] Heart rate variability: Standards of measurement, physiological interpretation, and clinical use. *Circulation*. 1996;93(5):1043-1065. DOI: 10.1161/01.CIR.93.5.1043.
[24] Shaffer F, Ginsberg JP. An overview of heart rate variability metrics and norms. *Frontiers in Public Health*. 2017;5:258. DOI: 10.3389/fpubh.2017.00258.
[25] De Godoy MF. Nonlinear analysis of heart rate variability: A comprehensive review. *Journal of Cardiology and Therapy*. 2016;3(3):528-533. DOI: 10.17554/j.issn.2309-6861.2016.03.101-4.
[26] Tarvainen MP, et al. Kubios HRV–heart rate variability analysis software. *Computer Methods and Programs in Biomedicine*. 2014;113(1):210-220. DOI: 10.1016/j.cmpb.2013.07.024.
[27] Brennan M, Palaniswami M, Kamen P. Do existing measures of Poincare plot geometry reflect nonlinear features of heart rate variability?. *IEEE Transactions on Biomedical Engineering*. 2001;48(11):1342-1347. DOI: 10.1109/10.959330.
[28] Xu C. *Design of a pulse wave based mental fatigue detection system*. PhD Thesis. Chongqing University of Technology, China; 2021. DOI: 10.27753/d.cnki.gcqgx.2021.000833.
[29] Wang CY, et al. Fatigue detection system based on indirect-contact ECG measurement. *2016 International Conference on Advanced Robotics and Intelligent Systems (ARIS)*. 2016. DOI: 10.1109/ARIS.2016.7886623.
[30] Zeng C, et al. Sex differences in time-domain and frequency-domain heart rate variability measures of fatigued drivers. *International Journal of Environmental Research and Public Health*. 2020;17(22):8499. DOI: 10.3390/ijerph17228499.
[31] Mourot L, et al. Quantitative Poincare plot analysis of heart rate variability: Effect of endurance training. *European Journal of Applied Physiology*. 2004;91(1):79-87. DOI: 10.1007/s00421-003-0917-0.

毕玖琚，秦训鹏，胡东锦，徐晨阳
基于成像光电容积描记法的疲劳驾驶检测方法

摘要
生理信号指标能准确反映疲劳程度，但接触式检测方法会对驾驶员的驾驶产生较大影响。本文提出了一种非接触式疲劳驾驶检测方法。使用摄像头和其他设备收集有关驾驶员面部的信息。记录一段时间内的面部变化并处理录制的视频，从中提取出脉搏波。然后根据脉搏波特征提取心率变异性的频域指标和非线性指标。最后，实验证明，该方法可以清晰地判断驾驶员是否疲劳。本研究采用成像光电容积描记法技术实现非接触式驾驶员疲劳检测，与通过识别驾驶员眨眼和打哈欠的非接触式检测方法相比，本文采用的生理信号更具说服力。与其他通过检测生理信号判断驾驶员疲劳程度的方法相比，该方法具有非接触、快速、方便等优点，适用于座舱环境。

关键词：
车辆安全系统；主动安全系统；智能座舱；疲劳检测；成像光电容积描记法